

Manufacturing of dies from hardened tool steels by 3-axis micromilling

Dirk Biermann · Alexander Baschin ·
Eugen Krebs · Juliane Schlenker

Received: 23 August 2010 / Accepted: 30 December 2010 / Published online: 13 January 2011
© German Academic Society for Production Engineering (WGP) 2011

Abstract In this paper the results of an experimental investigation to analyze the machinability of a hardened, carbide-rich cold-work tool steel 1.2379 (approx. 62 HRC) with coated micro end-milling cutters are discussed. Fundamental experiments were performed to determine a cutting-parameter set, which enables an economic manufacturing of dies by 3-axis micromilling with commercially available cemented-carbide tools. The evaluation of the applicability of different tool types is conducted by analyzing the process forces, the tool wear, the surface quality, the material removal rate, and the entire chip volume. Design of experiments was used to significantly reduce the number of experiments and to model the active and passive forces. Concerning the design of tools for the micromilling of such difficult-to-machine materials, it is shown that cemented-carbide tools with robust cutting edges are applicable for this kind of machining. Furthermore, test microstructures were manufactured with the intention of validating the determined cutting-parameter set in combination with the selected tool types. In addition, the dimension and shape accuracy of the microstructures are analyzed.

Keywords Micromilling · Dies · Hardened tool steel

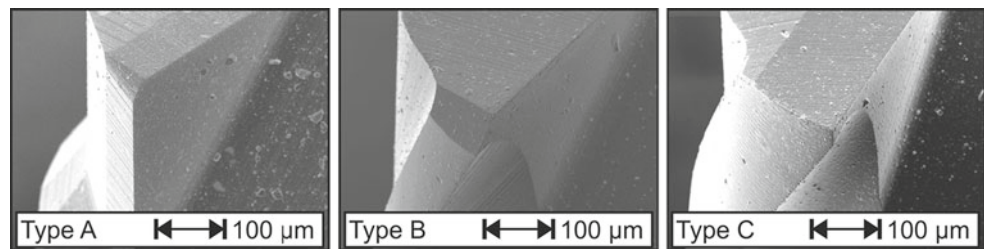
1 Introduction

Micromilling is a suitable technique for the manufacturing of forming dies from hardened tool steels with a high

quality with respect to the shape accuracy, the surface quality, and the wear resistance. The trend to form materials with increasing tensile strength and toughness, as well as sheet-bulk metals or microparts, results in the application of dies with a hardness above 50 HRC [1–6]. In macro dimensions, machining of hardened steels is a challenge for the application of cemented-carbide tools. Therefore, the utilization of super hard cutting materials, such as cBN, for machining hardened steels is state of the art [7–9]. In the range of micromilling, the manufacturing of cBN micro end-milling cutters by grinding allows the application of such tools for the micromilling of hardened steels [1, 10, 11]. However, the significantly higher price of cBN micro end-milling cutters compared to the ones consisting of submicron or fine-grain cemented carbide (sgcc or fgcc) is an argument against the application of these tools. As a result of this, the further development of geometries and coatings of sgcc and fgcc micro end-milling cutters led to promising results concerning the micromachinability of hardened tool steels. Li et al. developed micro end-milling cutters with two and four teeth for the micromilling of hardened tool steels (50–56 HRC). For the optimization of the design of the cutting edge corners and of the core shape of conventional tools, mechanical tool loads were analyzed with a FEM system [12]. The application of the new tool types in experiments led to lower tool wear and burr formation compared to the conventional tool type. The results of the experimental investigations, performed by Aramcharoen et al. showed that coated micro end-milling cutters with chamfered and rounded cutting edges lead to high surface quality and low burr formation when micromachining hardened tool steels with a hardness of 45 HRC [4, 5]. Furthermore, many experimental investigations deal with the machining of hardened (tool) steels by micromilling [13–15].

D. Biermann · A. Baschin (✉) · E. Krebs · J. Schlenker
Institute of Machining Technology, Technische Universität
Dortmund, Baroper Straße 301, 44227 Dortmund, Germany
e-mail: baschin@isf.de

Fig. 1 SEM micrographs of the cutting edges and specifications of the fgcc tools



Type	A	B	C
Coating	TiAlN	AlTiN	TiAlN
Tool length l_t	40 mm	50 mm	45 mm
Shank diameter d_S	3 mm	3 mm	3 mm
Number of teeth z	2	2	2
Diameter d	1 mm	1 mm	1 mm
Ratio l/d	0.5	1	2.5
Helix angle ϵ	0°	25°	30°
Rake angle γ	0°	10°	-
Corner radius r_ϵ	0.05 mm	45° chamfer	0 mm
Cutting edge radius r_β	ca. 6 μm	ca. 6 μm	ca. 7 μm

The goal of this experimental investigation is to show the applicability of commercially available sgcc micro end-milling cutters, which were designed for hard-milling operations, for the manufacturing of dies from a hardened cold-work tool steel with a hardness above 60 HRC and a high fraction of carbides. For the design of the micromilling process, it should be considered that a high material removal rate has to be achieved for an economic manufacturing of a die. Furthermore, it is very important to determine cutting parameters, which enable the roughing or finishing of a die with only one tool. This is a considerable criterion to achieve a high surface quality and shape accuracy. Previous investigations showed that micromilling of a high-speed steel (1.3343/HS6-5-2C, 63 HRC) with sgcc micro end-milling cutters leads to promising results concerning the material removal rate and the tool wear [16].

2 Experiments

2.1 Experimental setup

The experiments were carried out on a micromachining center, KERN HSPC 2522. The spindle used, Precise VSC 4084, has an operating range from 500 to 50,000 min^{-1} and a tool holder, HSK-E25, with a precision collet.

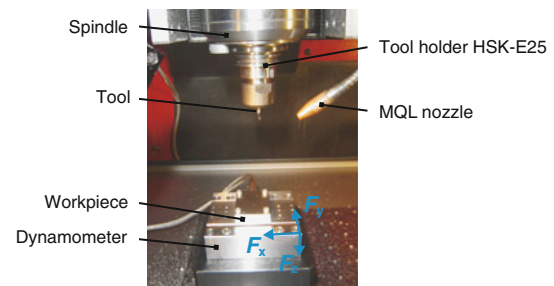


Fig. 2 Experimental setup

The investigations were performed by down milling with different types of micro end-milling cutters with a diameter of $d = 1$ mm. As a cooling and lubrication concept, minimum quantity lubrication (MQL) was chosen. The specifications of the tools are listed and the cutting edges are illustrated in Fig. 1. The experimental setup is depicted in Fig. 2. The forces were measured with a 3-component dynamometer, Kistler MiniDyn 9256C1, and were recorded with a sampling rate of $f_s = 50$ kHz. The workpiece material was a cold-work tool steel, 1.2379 (X153CrMoV12), with a hardness of approx. 62 HRC. The workpiece dimension was $30 \times 40 \times 10$ mm. A tool life travel path of $L_t = 1.5$ m for each cutting-parameter set was aimed for. Figure 3 shows pictures of the material structure, which exhibits a high fraction of

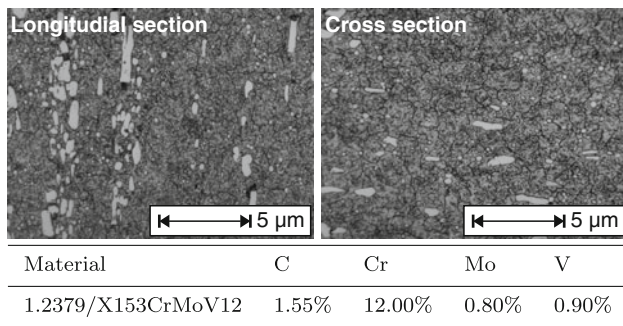


Fig. 3 Microstructure and nominal composition (wt%) of the hardened cold-work tool steel

inhomogeneously distributed carbides. The generated surfaces, microstructures and cutting edges of the tools were analyzed with the aid of a confocal white-light microscope, Nanofocus μsurf, and a scanning electron microscope (SEM), Philips XL40 ESEM. Furthermore, the maximum width of flank wear land VB_{max} was measured by light microscopy using a Mitutoyo MF-B 1720 H microscope. After the fundamental investigations with tool type A for the determination of a suitable cutting-parameter set, a comparative investigation with tool types A, B, and C was performed. Finally, for the validation of the cutting-parameter set, microstructures were manufactured from the hardened cold-work tool steel.

2.2 Design of experiments

The previous experiments, which dealt with the micromachining of a hardened high-speed steel (1.3343/HS6-5-2C, 63 HRC), established a cutting-parameter set and a tool type, which enable the machining of microstructures with an acceptable material removal rate, low tool wear, moderate process forces, and a good surface quality. Within these investigations, design of experiments was used to optimize this cutting-parameter set for tool type A for the manufacturing of microstructures from the hardened cold-work tool steel with a high fraction of inhomogeneously distributed carbides. Thus, this cutting-parameter set was selected as the center point of a central composite design and was repeated four times. Preliminary experiments for the determination of a suitable cutting speed were performed, and the obtained value of $v_c = 130$ m/min was kept constant during the following experiments. The cutting-parameter values were varied in the following ranges: depth of cut $a_p = 0.01, \dots, 0.04$ mm, width of cut $a_e = 0.2, \dots, 0.6$ mm, and feed per tooth $f_z = 0.01, \dots, 0.04$ mm. The sequence of the experiments was randomized with the intention of avoiding disturbances and trends due to the experimental procedure. The randomized design of experiments is listed in Table 1.

Table 1 Randomized experiments

No.	v_c (m/min)	f_z (mm)	a_p (mm)	a_e (mm)
1	130	0.025	0.025	0.400
2	130	0.016	0.016	0.519
3	130	0.025	0.025	0.200
4	130	0.016	0.016	0.281
5	130	0.025	0.040	0.400
6	130	0.034	0.016	0.519
7	130	0.010	0.025	0.400
8	130	0.025	0.025	0.600
9	130	0.025	0.025	0.400
10	130	0.016	0.034	0.519
11	130	0.025	0.025	0.400
12	130	0.025	0.025	0.400
13	130	0.034	0.034	0.281
14	130	0.034	0.034	0.519
15	130	0.040	0.025	0.400
16	130	0.025	0.010	0.400
17	130	0.034	0.016	0.281
18	130	0.025	0.025	0.400
19	130	0.016	0.034	0.281

The center point experiments of the central composite design are shown in bold

3 Fundamental investigations

In this section the results of the fundamental investigations are presented. First, the models of the active and passive forces are described, and the significance of the factors depth of cut, width of cut, and feed per tooth is analyzed. After this, a suitable cutting-parameter set is determined by analyzing the tool wear, the surface quality of the generated microstructures, the achievable entire chip volume, and the material removal rate.

3.1 Analysis of active and passive forces

Concerning the avoidance of tool or cutting edge breakage, the consideration and analysis of the forces is indispensable. Figure 4 shows the models of the averaged active forces for the analysis of the interactions between depth of cut and feed per tooth as well as between width of cut and depth of cut (coefficient of determination $R_{adj}^2 = 0.972$). As expected, the models suggest a significant influence of the depth of cut on the active forces due to the correlation between the depth of cut and the width of undeformed chip. The width of cut and the feed per tooth have a low influence on the active forces in the range of low and middle-sized values of the depth of cut. Figure 5 shows the models of the averaged passive forces for the analysis of the interactions between depth of cut and feed per tooth as

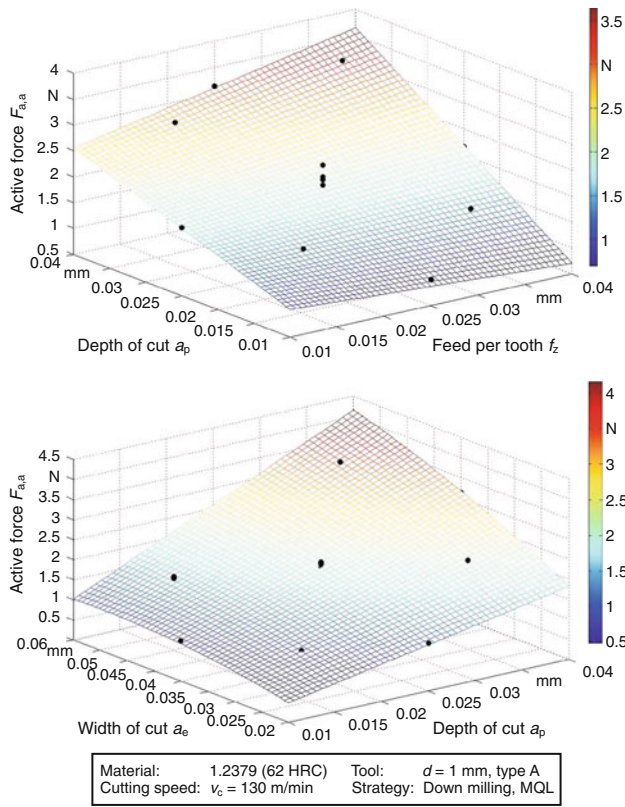


Fig. 4 Models of the averaged active forces for constant cutting speed v_c depending on depth of cut a_p , width of cut a_e , and feed per tooth f_z

well as between width of cut and depth of cut. The progression of the passive force models clarifies that a reduction of the cross-section of undeformed chip leads to an increase of the passive forces due to ploughing effects. In this case, by means of the coefficient of determination of $R^2_{adj} = 0.436$, it is clear that the modeling of passive forces for micromilling is very difficult because there are many disturbances, which influence the micromilling process. On the one hand, the determination of the zero position in height by scratching the workpiece with the rotating tool can lead to uneven wear of the minor cutting edges of the tool and, on the other hand, the condition of the cutting edges of each tool differs due to the manufacturing and the coating of the tools. Therefore, there is a strong mean variation of the passive forces. In contrast to the passive forces, the modeling of the active forces leads to good results.

For the determination of a suitable cutting-parameter set, an analysis of the interactions between the factors by considering the coefficients of the regression equations is essential (Table 2). Due to the high weighting of the depth of cut in combination with the other factors in the regression equations, an increase of the depth of cut leads to a significant increase of the forces. The increase of the width of cut in the range of small and middle-sized depths of cut

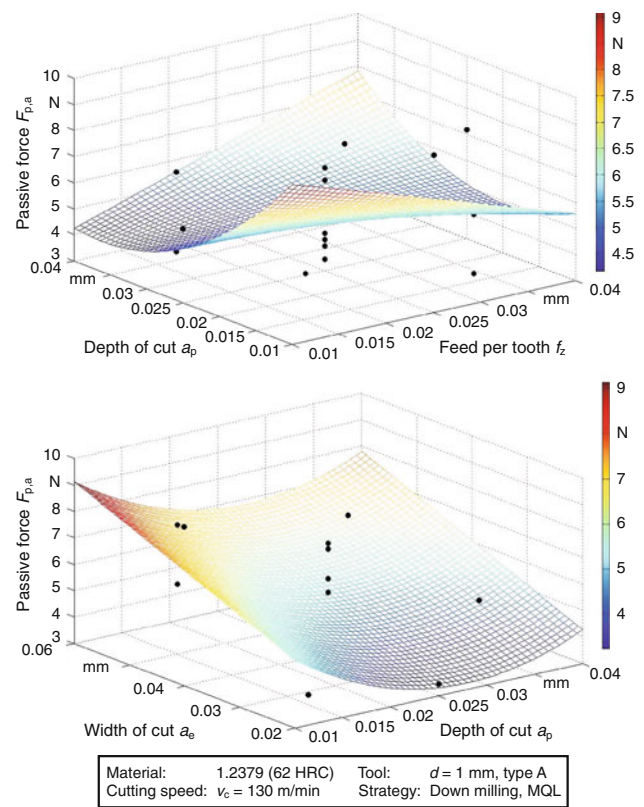


Fig. 5 Models of the averaged passive forces for constant cutting speed v_c depending on the depth of cut a_p , width of cut a_e , and feed per tooth f_z

Table 2 Comparison of the regression coefficients of the active and passive force models

Factors and interactions	F_a	F_p
f_z	0.18999	–
a_p	1.11	–0.65162
a_e	0.72	1.7703
$f_z * a_p$	0.35796	1.785
$a_p * a_e$	0.45331	–
$a_p * a_p$	–0.17869	1.6187

leads to a moderate increase of the active force. In this case, the adjustment of large widths of cut in the micromilling process is reasonable.

3.2 Tool wear, material removal rate, entire chip volume, and surface quality

Due to the different cutting-parameter sets in addition to the defined tool life travel path of $L_t = 1.5$ m (50 paths) in this investigation, the analysis of the maximum width of flank wear land VB_{max} is difficult because each experiment leads to different material removal rates Q_w and entire chip

Table 3 Experiments classified with regard to the entire chip volume Q and the maximum width of flank wear land VB_{max} (best-in-class principle)

No.	VB_{max} (μm)	Q_w (mm^3/min)	Q (mm^3)	Group no.
16	39.50	8.200	6.000	1
17	41.10	12.572	6.780	2
4	43.45	5.960	6.780	2
3	36.55	10.250	7.500	3
6	36.90	23.210	12.517	4
2	45.55	11.004	12.517	4
19	42.45	12.572	14.301	5
13	56.60	26.517	14.301	5
1	35.40	20.500	15.000	6
7	45.90	8.200	15.000	6
9	35.70	20.500	15.000	6
11	38.60	20.500	15.000	6
12	46.30	20.500	15.000	6
15	36.90	32.800	15.000	6
18	45.40	20.500	15.000	6
8	38.45	30.750	22.500	7
5	40.55	32.800	24.000	8
10	42.35	23.210	26.402	9
14	39.75	48.955	26.402	9

volumes Q . The aim of this investigation was to determine a cutting-parameter set which enables the roughing of a die or microstructures with one tool in an adequate time. This means that tool wear has to be evaluated concerning the main criterion Q and the additional criterion Q_w . In this case, the experiments are classified (best-in-class principle) with respect to Q (Table 3). The listed results of the maximum width of flank wear land VB_{max} are averaged values of the two teeth of each tool.

The experiments number 1, 3, 5, 6, 8, 14, 16, 17, and 19 offer the best cutting-parameter sets in their classes. For the determination of a suitable cutting-parameter set, a graphical comparison of the criteria simplifies the comparison of the achieved results (Fig. 6). Due to the goal of this investigation, favorable cutting-parameter sets lead to low tool wear and high entire chip volumes. A criterion for the evaluation of the results is the average value $VB_{max,a} = 41.4 \mu\text{m}$ for all experiments. As a result of this, experiment number 19 with $VB_{max,a} = 42.45 \mu\text{m}$ is dropped from the favorable group of cutting-parameter sets. The experiments number 1 and 6 led to similar values with regard to Q_w and Q , but experiment number 6 is preferred due to the lower tool wear. Furthermore, this reason is also the basis for the preference of experiment number 3 compared to number 16 and 17. Due to the high values for Q_w , Q , and $VB_{max} < VB_{max,a}$, the experiments number 5, 8, and 14 will

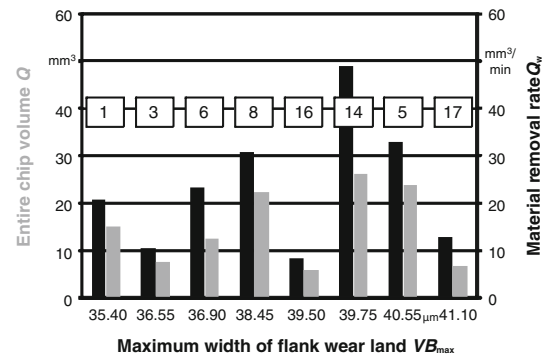


Fig. 6 Comparison of the maximum width of flank wear land VB_{max} , the material removal rate Q_w , and the entire chip volume Q for eight selected experiments

Table 4 Comparison of the arithmetical mean deviation of the roughness profile S_a , the average surface roughness R_z , and the burr height for five selected experiments

No.	S_a (μm)	R_z (μm)	Burr height (μm)
1	0.318	1.990	5.11
3	0.536	1.886	–
5	0.422	2.453	23.29
8	0.298	1.945	4.85
14	0.358	2.190	5.87

be considered in addition to the experiments number 1 and 3 for further analyses.

The surface quality is characterized by the arithmetical mean deviation of the roughness profile S_a and the average surface roughness R_z of the last milling path. The burr height, measured at the flank of the last milling path, is a further criterion for the evaluation of the microstructure quality. The consideration of Table 4 demonstrates that cutting-parameter sets from the experiments number 1 and 8 lead to the highest surface quality and the lowest burr formation.

3.3 Short summary

Taking all criteria into account, this investigation leads to the result that the cutting-parameter set of experiment number 8 ($v_c = 130 \text{ m/min}$, $f_z = 0.025 \text{ mm}$, $a_p = 0.025 \text{ mm}$, and $a_e = 0.6 \text{ mm}$) is suitable for an economic manufacturing of dies. The determined cutting-parameter set differs from the center point of the design of experiments concerning the width of cut. An increase of the width of cut from $a_e = 0.4 \text{ mm}$ to $a_e = 0.6 \text{ mm}$ leads to an excellent surface quality and a significantly shorter processing time. Furthermore, it is evident that the modeling of passive forces for micromilling processes is very difficult due to

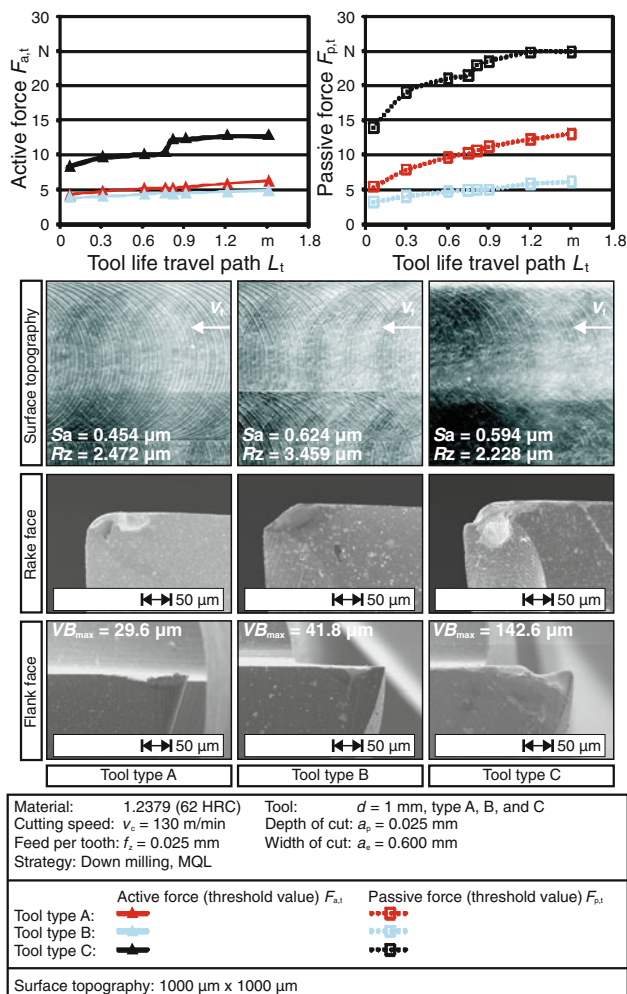


Fig. 7 Active and passive forces (threshold value) $F_{a,t}/F_{p,t}$ depending on the tool life travel path L_t , micrographs of the surfaces and the tools

the high mean variations of the measured forces in the experiments.

4 Applicability of different tool types

Within this investigation, experiments with the tool types A, B, and C were performed with the intention to analyze the optimization potential of the determined cutting-parameter set. Therefore, three attempts with three tools of each type were carried out in order to identify the mean variations of the results. Figure 7 shows the active and passive forces depending on the tool life travel path as well as micrographs of the surface topographies and of the tools. The figure shows that the application of tool type B with a positive rake angle of $\gamma = 10^\circ$ leads to the lowest active and passive forces. For tool type A with a neutral rake angle, the trend of the forces is similar whereas the level of the passive force is higher. The application of tool type C

leads to high forces in addition to an irregular progression depending on the tool life travel path. The SEM micrographs of the rake and the flank face of tool type C illustrate that the tool wear is significantly higher in comparison to the tool types A and B. Due to the large helix angle of $\epsilon = 30^\circ$ and the unprepared corner, the stability of the cutting edge is reduced and tool wear is accelerated. Furthermore, the neutral rake angle and the nonhelical cutting edges of tool type A compared to the positive rake angle and the helical cutting edges of tool type B result in negligibly higher forces, but lower tool wear. At first glance, micromilling with tool type C leads to an acceptable surface quality concerning the arithmetical mean deviation of the roughness profile S_a and the average surface roughness R_z . However, the quality of the generated surfaces is poor because the worn cutting edges of the tool smear the removed material. The best surface quality follows from the application of tool type A. Unexpectedly, the characteristic values of the surface generated by tool type B suggest a bad surface quality due to the distinct characteristic structure of the milling process in the areas where the teeth engage into the workpiece. Due to the length of this tool type and the low stiffness, this fact is a hint for a strong tool deflection in the process, which affects the surface quality. Based on these results, microstructures were manufactured with tool type A and B.

5 Manufacturing of microstructures

Micromilling with the suitable cutting-parameter set in addition to the tool life travel path of $L_t = 1.5$ m led to a material removal of an entire chip volume of $Q = 22.5$ mm³ and low tool wear. As a result of this, the targeted entire chip volume for the manufacturing of test microstructures was increased to $Q = 40.53$ mm³ and the depth of cut was reduced by 0.005 mm. The two test microstructures are an area with four webs and a pyramid consisting of three stacked blocks, pictured in Fig. 8. The 3-axis tool paths were generated by the CAM-software Cimatron E8.5. The strategy was spiral machining, and the machining type was roughing.

The evaluation of the surface quality of the web area is conducted by means of the characteristic values arithmetical mean deviation of the roughness profile S_a and average surface roughness R_z . Figure 9 shows that the arithmetical mean deviation of the roughness profile is very low for both tool types, where the values for tool type A are insignificant lower. For the average surface roughness, which clearly indicates grooves and scratches on the surface, there is a significant difference between the value levels of tool type A and B. The analysis of the dimensional and shape accuracy of the generated test

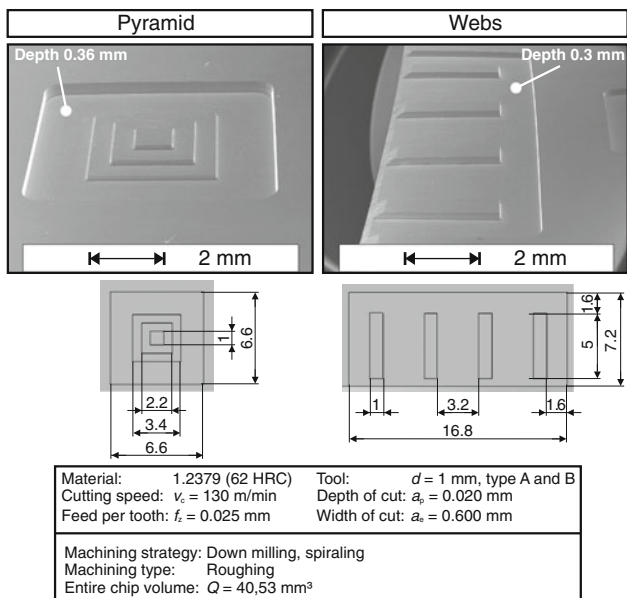


Fig. 8 SEM micrographs and geometrical dimensions of the test microstructures

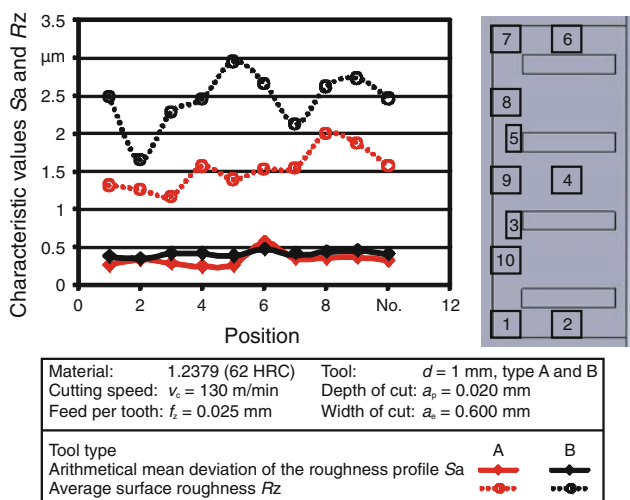


Fig. 9 Measured arithmetical mean deviation of the roughness profile Sa and average surface roughness Rz of the web area

microstructures reveals more discrepancies concerning the suitability of tool type B in addition with this cutting-parameter set. Figures 10 and 11 illustrate SEM micrographs of the web area and the pyramid. In the area of the webs, where the tool leaves the workpiece (Fig. 10a), surface location errors occur due to the dynamic behavior of the tool. Particularly, in the corners of the web area (Fig. 10c). Here, the immersion angle increases and chatter occurs, which results in chatter marks on the flank. At the pyramid, surface location errors occur at the flanks of the blocks due to tool deflections (Fig. 11a, b). As in the previous experiments, it is evident that the application of tool

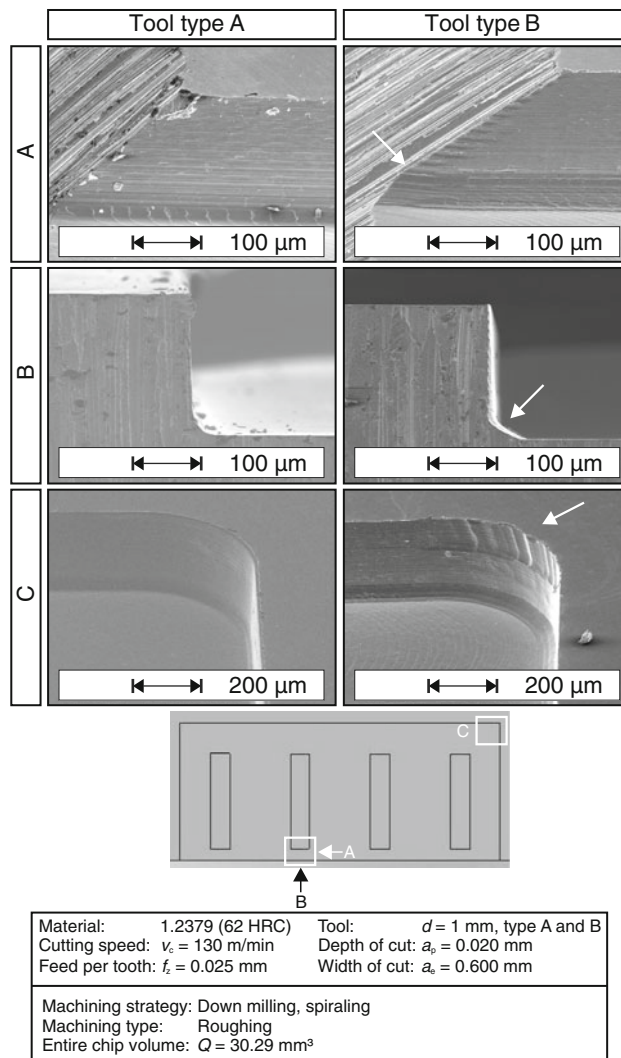


Fig. 10 SEM micrographs of the web area manufactured with tool type A and B

type B leads to a distinct surface structure due to the stronger tool deflection compared to tool type A (Fig. 11c). Furthermore, the chamfer at the cutting edge corner of tool type B generates landings at the structures, e.g. Fig. 11c, in contrast to tool type A, which has a small corner radius of $r_c = 0.05$ mm. Smeared workpiece material, illustrated on the micrographs in Fig. 11c, clarifies a general problem of the micromilling process with small undeformed chip thicknesses. At the outer edges of the webs and blocks, the feed velocity is reduced and the material is smeared on the surface of the workpiece due to ploughing effects, which lead to a poor surface quality and an accelerated tool wear. With respect to the tool wear, both tool types exhibit an acceptable maximum width of flank wear land VB_{max} of approximately $65 \mu\text{m}$. However, the increasing tool wear in the process leads to an undesirable burr formation at the microstructures, although the burr formation in the

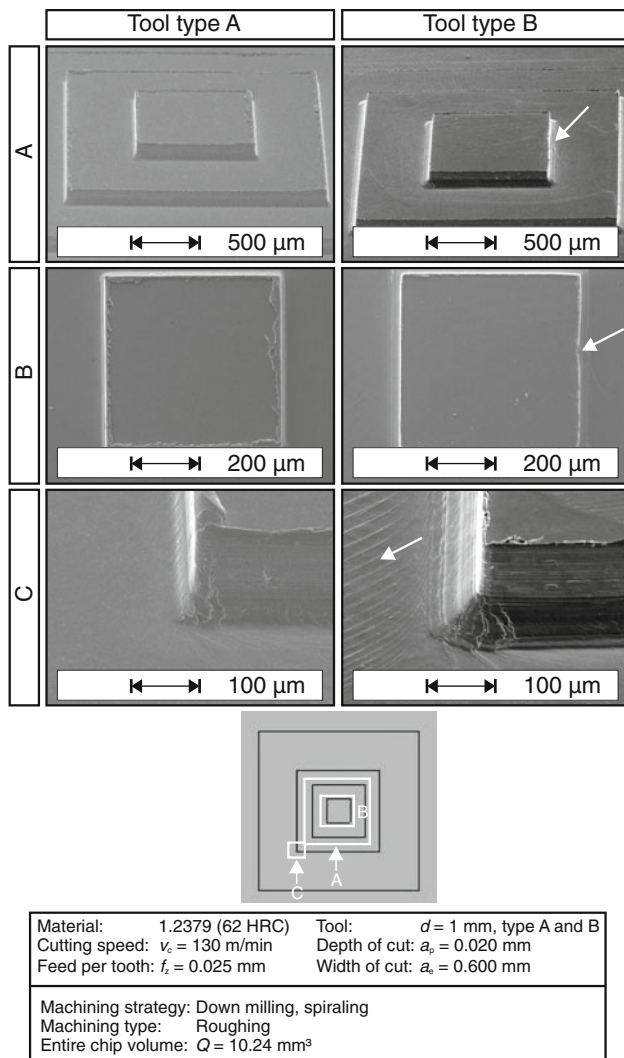


Fig. 11 SEM micrographs of the pyramid manufactured with tool type A and B

fundamental experiments was negligible. The reasons for this result are the changing tooth engagement conditions and the variable undeformed chip thicknesses in the NC micromilling process, which lead to stronger wear at the minor and the major cutting edges. The results of this investigation show that a simple transfer from the knowledge of the fundamental investigation to the NC micromilling processes is not possible.

6 Conclusions and outlook

The results of the experimental investigations presented in this paper show that an economic manufacturing of dies from a hardened cold-work tool steel with cemented-carbide micro end-milling cutters is possible. In this case, with regard to the criteria tool life travel path, material removal

rate, entire chip volume, surface quality, and shape accuracy, the application of tool type A leads to promising results so that the application of expensive micro end-milling cutters consisting of cBN is not necessary. Furthermore, the results show that the design of the tool is essential in the range of micromilling of steels with a hardness above 60 HRC. The best results were achieved with tool type A, which has nonhelical cutting edges, a small corner radius, and a neutral rake angle. Due to the high stiffness, the low tool length and aspect ratio, the applied forces lead to negligible tool deflections and vibrations. In contrast to this fact, the application of tool type B, which is 10 mm longer than tool type A, results in undesirable surface location error and a poor surface quality due to tool deflections and vibrations.

The goal of future investigations is the adaptation of the cutting parameters for the manufacturing of more delicate structures from hardened tool steels with smaller micro end-milling cutters (e.g. $d = 0.4$ mm) and the analysis of the finishing of microstructures. Furthermore, experiments with ball end-milling cutters and different tool inclinations in feed and cross-feed direction will be performed with the intention of realizing the transfer from 3-axis to 5-axis micromilling of hardened tool steels.

Acknowledgments This article is based on investigations of the research project B2 “Machining of molds with filigree structures for sheet-bulk metal forming”, which is kindly supported by the German Research Foundation (DFG) within the SFB/TR 73.

References

- Klocke F, Bergs T, Veselovac D, Arntz K, Quito FJ, Kratz S (2007) Von der Makro-zur Mikrowelt. Herausforderung für den Mikroformenbau. *Wt Werkstattstechnik* 97(11/12):842–846 (online)
- Klocke F, Arntz K, von Bodenhausen J (2004) Potenzial beim Hartfräsen von Mikrostrukturen. *Mikroproduktion* (1):24–26
- Fleischer J, Löhle D, Kotschenreuther J, Schulze V, Deuchert M, Halvadjiysk G, Haupt S, Kienzler A (2007) Fertigungsverfahren in der Mikrotechnik. Oberflächenqualität und Miniaturisierungspotenzial von Mikroformmeinsätzen. *Wt Werkstattstechnik* 97(11/12):847–851 (online)
- Aramcharoen A, Mativenga PT (2009) Size effect and tool geometry in micromilling of tool steel. *Precis Eng* 33(4):402–407
- Aramcharoen A, Mativenga PT, Yang S, Cooke KE, Teer DG (2008) Evaluation and selection of hard coatings for micro milling of hardened tool steel. *Int J Mach Tools Manuf* 48(11/12):1578–1584
- Eichenhüller B, Engel U, Geiger M (2010) Microforming and investigation of parameter interactions. *Prod Eng Res Dev* 4(2/3):135–140
- Sieben B, Wagner T, Biermann D (2010) Empirical modeling of hard turning of AISI 6150 steel using design and analysis of computer experiments. *Prod Eng Res Dev* 4(2/3):115–125
- Denkena B, Boehnke D, Meyer R (2008) Reduction of wear induced surface zone effects during hard turning by means of new tool geometries. *Prod Eng Res Dev* 2(2):123–132

9. Klocke F, Brinksmeier E, Weinert K (2005) Capability profile of hard cutting and grinding processes. *CIRP Ann Manuf Technol* 54(2):22–45
10. Suzuki H, Kimura T, Yamamoto Y, Moriwaki T, Okino T, Hijikata Y, Goto I, Goto T, Ono T, Goto Y, Isono H, Takahashi N (2005) Micro milling of hard material with micro milling tool. In: *Proceedings of the 5th international conference of the EUSPEN*, 8–11 May 2005, Montpellier, France, pp 577–580
11. Arntz K, Quito EF (2007) Hartfräsen von Mikrostrukturen—zukunftsweisend für den Präzisionsformenbau. *Der Stahlformenbauer* (6):124–126
12. Li P, Hoogstrate AM, Oosterling JAJ, Langen HH, Munnig Schmidt R (2008) Experimental validation of micro endmill design for hard milling application. In: *Proceedings of the 3rd international CIRP high performance cutting conference*. 12–13 June 2008, Dublin, pp 69–78
13. Kahnis P (2008) Analyse von Größeneinflüssen bei der Herabskalierung des Fräsprozesses in den Mikrobereich. Dissertation, Technische Universität Dortmund
14. Hüntrup V (2000) Untersuchungen zur Mikrostrukturierbarkeit von Stählen durch das Fertigungsverfahren Fräsen. Dissertation, Universität Karlsruhe
15. Schauer K (2006) Entwicklung von Hartmetallwerkzeugen für die Mikrozerspanung mit definierter Schneide. Dissertation, Technische Universität Berlin
16. Biermann D, Kahnis P (2010) Mikrofräsen filigraner Strukturen in Formeinsätzen. *MM Maschinenmarkt* (5):36–40